PAPER

Check for updates

Construction of carbon dots/metal–organic framework composite for ratiometric sensing of norfloxacin†

Shixin Wu,[a] Chun Chen,[a] Jiahao Chen,[a] Wei Li,[a] Minhua Sun,[a] Jiechun Zhuang,[a] Junjie Lin,[a] Yingliang Liu, [ID][a] Hong Xu,[a] Mingtao Zheng, [ID] *[ab] Xuejie Zhang, [ID] [ab] Bingfu Lei [ID] *[ab] and Haoran Zhang*[ab]

Quinolone antibiotics such as norfloxacin (NFX) are widely used to treat many bacterial infections, but antibiotic residues in water and food will worsen the pathogenesis of resistant bacteria, and long-term use of antibiotics leads to drug resistance. Hence, we designed and synthesized the composite of green carbon dots and UiO-66 (g-CDs@UiO-66) as a fluorescent sensing material by integrating carbon dots, which are rich in hydroxyl and carboxyl groups, into the zirconium-based metal–organic framework UiO-66 through the solvothermal method. This composite possesses the excellent optical properties of g-CDs and the selective response and the enrichment of UiO-66 to the target analytes, which can be applied to the detection of norfloxacin in milk and pork samples. The results prove that g-CDs@UiO-66 shows a good performance in the detection of norfloxacin with a limit of detection (LOD = 0.082 μM) in the linear range of 1–8 μM. Further research indicates that the presence of strong hydrogen bonds between g-CDs@UiO-66 and norfloxacin is the main reason for the fluorescence enhancement, and provides a new approach to the development of fluorescent nanosensing technology in the field of food and environmental safety inspection.

Introduction

Norfloxacin (NFX) is one of the third-generation quinolone antibiotics known as fluoroquinolones (FQs), which have been applied widely to the treatment of clinical infection and as antibacterial drugs due to its positive effects such as the inhibition of cellular DNA cyclase, inhibition of DNA replication, the killing of bacteria and the treatment of skin infections.[1,2] However, antibiotics are considered to be a new environmental contaminant due to their persistence in the natural environment and injury to organisms. For instance, the continued intake of antibiotics by humans can lead to other human health problems such as weakened immunity, allergic reactions, hereditary diseases, and the occurrence of cancer. Until now, a number of methods have been developed for the determination of NFX

residues, such as liquid chromatography with fluorescent detection,[3] sequential injection analysis,[4] high-performance liquid chromatography,[5] capillary electrophoresis,[6] and electrochemical analysis.[7] Among them, liquid chromatography with fluorescent detection can achieve good sensitivity, but the pretreatment step required is time-consuming and the equipment is expensive. Capillary electrophoresis enables microdetection, but the reproducibility and sensitivity of the separation are poor. In addition, electrochemical detection offers a wide range of concentrations but poor selectivity. It is essential to develop a fast, efficient, sensitive, and specific detection technique for the detection of antibiotics in food samples.[8]

Metal–organic frameworks (MOFs), are porous materials composed of metal ions/clusters and organic linkers, which have been widely used in gas storage and separation,[9] catalysis,[10,11] drug delivery,[12] luminescent sensing[13,14] and other fields owing to its characteristics of high specific surface area and controllable surface engineering. Within this large family, zirconium-based MOFs represented by UiO-66 (UiO = University of Oslo) have the advantages of high coordination, high thermal stability, a large specific surface area, and low toxicity, promoting Zr-MOFs into the field of inspection applications to remove various contaminants in wastewater.[15] Due to their modularity, functionality, high sensitivity, and specificity for target analyte detection, MOFs

[a] *Key Laboratory for Biobased Materials and Energy of Ministry of Education, College of Materials and Energy, South China Agricultural University, Guangzhou 510642, P. R. China. E-mail: mtzheng@scau.edu.cn, tleibf@scau.edu.cn, hrzhang@scau.edu.cn*

[b] *Maoming Branch, Guangdong Laboratory for Lingnan Modern Agriculture, Guangdong Maoming 525100, P. R. China*

† Electronic supplementary information (ESI) available. See DOI: https://doi.org/10.1039/d2tc03414j

are rapidly developing as fluorescent sensor materials.[16,17] By combining pre-designed multi-tooth organic coupling agents with an appropriate selection of metal ions, or by adding suitable emission-detection molecules, the fluorescence and sensing properties of MOFs can be adjusted in various ways. For instance, the fluorescence intensity, quantum efficiency, and stability of the metal framework of MOFs can be improved by introducing π-conjugated rigid organic binders.[18]

Over the past decade, fluorescence-based sensors have attracted wide attention for their high sensitivity, simple operation, and rapid response times. There have also been many reports focusing on fluorescent sensing properties based on MOFs, especially in indirect fluorescence detection, because MOFs have the following obvious advantages: (i) MOFs can selectively adsorb target analytes to improve the detection sensitivity; (ii) MOFs have developed active metal sites and Lewis sites that can facilitate binding to analytes to improve their detection selectivity; and (iii) the fluorescence properties of MOFs can be easily adjusted by utilizing the different origins of the MOF's luminescence center.[18] Most importantly, non-fluorescent substances can be detected by adding a second or third substance to produce indirect fluorescence properties, which significantly expands the type of analyte. MOFs are widely used as sensors, but their fluorescence performance is primarily derived from lanthanide-based metal ions and complex organic binders, which makes them difficult to prepare. In order to overcome this problem, host–guest assembly methods have been rapidly developed in which the fluorescent guest species is encapsulated into the cavities of the metal framework material to prepare metal–organic frame composite materials.[19,20] The adjustable pore size and ultra-high specific surface area make MOFs an excellent substrate for encapsulating a wide range of guest substances, such as carbon dots, fluorescent dyes, and various quantum dots.[18] As a promising new class of carbon nanomaterials, carbon dots are widely used in various fields such as catalysis, sensing, and bioimaging due to their excellent photoluminescence properties.[21–23] Compared with conventional phosphors, such as fluorescent dyestuffs and nanocrystals, CDs have the advantages of good biocompatibility, easy synthesis and functionalization, excellent water solubility, and chemical stability (photobleaching resistance).[24,25] In this work, the g-CDs@UiO-66 composite material with an excellent optical performance was constructed. The synthesized g-CDs@UiO-66 simultaneously inherits the luminescence performance of g-CDs and UiO-66, and exhibits good structural stability and fluorescence stability in aqueous solution. Based on the luminescence behavior of g-CDs@UiO-66, norfloxacin in milk and pork can be analyzed with high selectivity using the prepared g-CDs@UiO-66 as a fluorescent probe, showing a detection limit as low as (0.082 μM). Furthermore, we clarify that the existence of strong hydrogen bonds is the main reason for the fluorescence-enhancement phenomenon. As a result, the proposed fluorescent sensing materials show an excellent detection performance against norfloxacin, providing a new research platform for norfloxacin sensing.

Experimental

Materials

All reagents were purchased from Macklin Biochemical Technology Ltd. (Shanghai, China).

Characterization

A Hitachi F-7000 fluorescence spectrophotometer was used for fluorescence measurements. UV-Vis spectra were collected using a Shimadzu UV-2550 spectrofluorometer. The surface morphology of the samples was observed using a field emission scanning electron microscope (SEM; EVO MA 15). Transmission electron microscopy (TEM) images were obtained using an FEI Talos F200s electron microscope. Fourier transform infrared (FT-IR) spectra were obtained using a Thermo Fisher (Nicolet IS10) spectrometer. X-Ray photoelectron spectroscopy (XPS) spectra were obtained using an X-ray photoelectron spectrometer (Thermo Scientific K-Alpha^{+}).

Synthesis of green carbon dots (g-CDs)

First, 250 mg of riboflavin was dissolved in 40 mL of anhydrous ethanol and sonicated for 20 min.[26] The solution was transferred to an autoclave lined with PTFE and reacted for 10 h at 180 °C. After being cooled to room temperature, the solid impurities were removed via filtration through a 0.22 μm filter membrane and dialyzed at room temperature for 12 h (M_{w} = 1000 Da). Finally, the sample was obtained after freeze-drying.

Synthesis of UiO-66

UiO-66 was synthesized with modifications reported in the literature.[27,28] First, zirconium tetrachloride (70 mg) and benzoic acid (2.0 g) were dissolved in 8 mL DMF and sonicated for 10 minutes. The mixed solution was transferred to an oil bath and reacted for 1 h at 100 °C. After cooling to room temperature, 52 mg p-phthalic acid (PTA) and 52 μL trifluoroacetic acid (TFA) were added and reacted for 48 h at 120 °C, and the mixture was allowed to cool naturally to room temperature. The precipitate formed was centrifuged and washed several times with anhydrous ethanol and water. Later on, the obtained materials were dried for 12 h at 80 °C and finally calcined at 200 °C for 2 h using a muffle furnace.

Synthesis of the green carbon dots@UiO-66 (g-CDs@UiO-66) composite

300 mg of UiO-66 powder was dispersed in 10 mL green carbon dots solution and stirred for 12 h at 60 °C. The green precipitate was collected via centrifugation at 10 000 rpm for 10 min, and a green powder was obtained by drying at 80 °C for 12 h.

Selectivity of norfloxacin

All fluorescence measurements were carried out using the same method: g-CDs@UiO-66 was dispersed in DI water to obtain a stock solution (4 mg mL^{-1}). 300 μL (4 mg mL^{-1}) g-CDs@UiO-66 solution was added dropwise to 1 mL of PBS buffer at pH = 7.4 and reacted at ambient temperature for 10 min. A standard solution of 200 μL of different drug molecules was mixed with

This journal is © The Royal Society of Chemistry 2022

J. Mater. Chem. C, 2022, **10**, 15508–15515 | **15509**

the above mixture, incubated for 30 min, and fluorescence measurements were performed. The fluorescence emission spectrum was obtained at an excitation wavelength of 380 nm.

Application in real milk and pork samples

In practical applications, the feasibility and reliability of the carbon dot composite sensor were investigated, and milk and pork acquired at the South China Agricultural University supermarket were used as actual samples. Milk samples were pre-treated according to conventional reports,[29] 10 mL of milk was added to an admixture of methyl cyanide and distilled water (V/V = 4 : 1). The mixture was shaken manually for 3 min, followed by centrifugation at 10 000 rpm for 10 min to remove the protein precipitate and the resulting supernatant was diluted 10-fold. PBS buffer (pH = 7.4) and norfloxacin were added to the above milk solution to obtain a milk sample to be measured. The pork sample was also prepared as above.

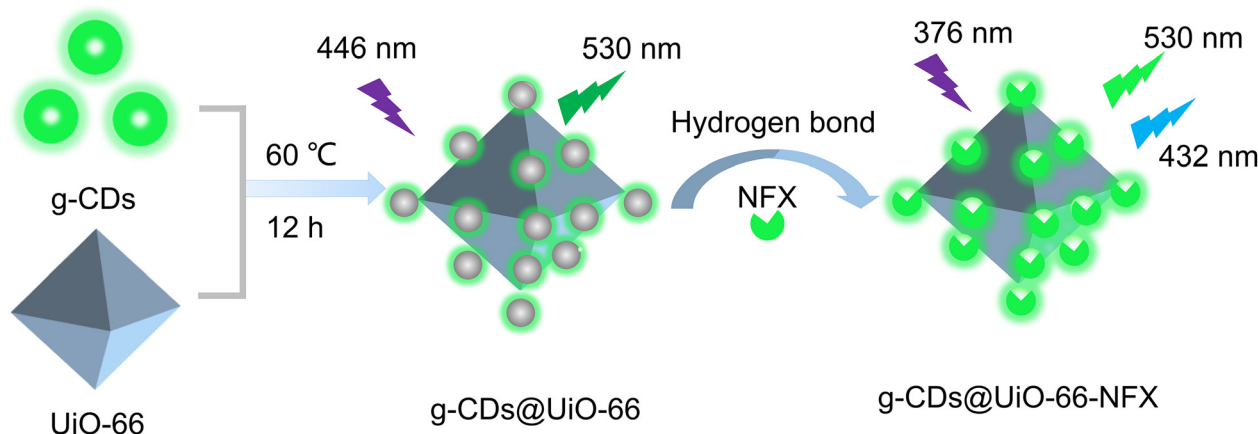## Results and discussion

Characterization of g-CDs, UiO-66 and g-CDs@UiO-66

To confirm the successful synthesis of UiO-66, the structure of UiO-66 was characterized using powder X-ray diffraction (XRD). As displayed in Fig. S1 (ESI†), the XRD patterns of UiO-66 coincided with the simulated peaks of UiO-66, demonstrating that the synthesis of UiO-66 was successful.[30] Scheme 1 depicts the synthesis process of the g-CDs@UiO-66 composite, in which the g-CDs@UiO-66 was prepared directly by incorporating g-CDs into the UiO-66 structure. Due to the abundant groups on the surface of the g-CDs, they are able to interact with the carboxyl group (COOH) on the surface of NFX, increasing the ability of the fluorescent material to detect norfloxacin.[31] When the g-CDs are compounded with UiO-66, the g-CDs@UiO-66 composite is rich in carboxyl and hydroxyl groups, forming strong hydrogen bonds with norfloxacin, resulting in an enhanced emission intensity.

To demonstrate the successful preparation of the g-CDs@UiO-66 composite material, characterization of the morphology of the materials was carried out via transmission electron microscopy

(TEM) and scanning electron microscope (SEM). As depicted in Fig. 1a, g-CDs are spherical and well dispersed with a broad grain-size range of 1.5–3.5 nm (Fig. 1b). It can be seen from the HRTEM images that the g-CDs have distinct lattice fringes with a lattice spacing of 0.21 nm (Fig. 1c), the g-CDs@UiO-66 composite material has a crystal structure with a lattice spacing of 0.21 nm, and 0.31 nm, which may be due to the (100) plane of graphite[32] and the (110) crystal plane of UiO-66, confirming the successful implantation of g-CDs into the UiO-66. The SEM images of UiO-66 shown in Fig. S2 (ESI†) exhibit regular *ortho*-octahedra with sizes in the range of 600–900 nm. After adding g-CDs, the surface morphology does not change but becomes relatively rough.[33] Moreover, the surface charge of the g-CDs and UiO-66 was examined by measuring the Zeta potential, which was −8.2 mV and +21.9 mV, respectively (Fig. S3, ESI†). Thus, it is safe to conclude that the synthesis of g-CDs and UiO-66 is linked in part *via* electrostatic interactions.[30]

To further clarify the chemical structure of CD-based composite materials, FT-IR, XRD, and XPS of the g-CDs, UiO-66, and g-CDs@UiO-66 composite material were carried out. Fig. 2a shows the XRD patterns of g-CDs@UiO-66 and its components. When g-CDs were compounded with UiO-66, the positions of the characteristic peaks of UiO-66 did not change obviously, which confirmed that the doping of g-CDs did not affect the original structure and crystallinity of UiO-66.[34] It is likely that the low concentration of g-CDs doped in the composite material is responsible for the absence of g-CD peaks in the XRD spectrum of the composite material. The bands and functional groups of the particles were characterized *via* their FT-IR spectrum (Fig. 2b). In comparison with g-CDs, the characteristic peaks of UiO-66 are observed in the g-CDs@UiO-66 particles. The 1650 cm^{-1} feature band of UiO-66 corresponds to the C=O stretching vibration of the carboxyl group and the O–C–O asymmetric contraction vibration. The 1506 cm^{-1} band represents the typical framework oscillation of a benzene ring.[35] The 658 cm^{-1} band is a Zr–O telescopic vibration throughout the UiO-66 unit.[36,37] In comparison with the spectra of g-CDs and UiO-66, the composite material has corresponding characteristic peaks at 3450, 2985, 1580–1660, 1506, 1154, and 658 cm^{-1}.

Scheme 1 Schematic representation for the preparation of g-CDs@UiO-66 and its application in norfloxacin sensing.

15510 | *J. Mater. Chem. C*, 2022, **10**, 15508–15515

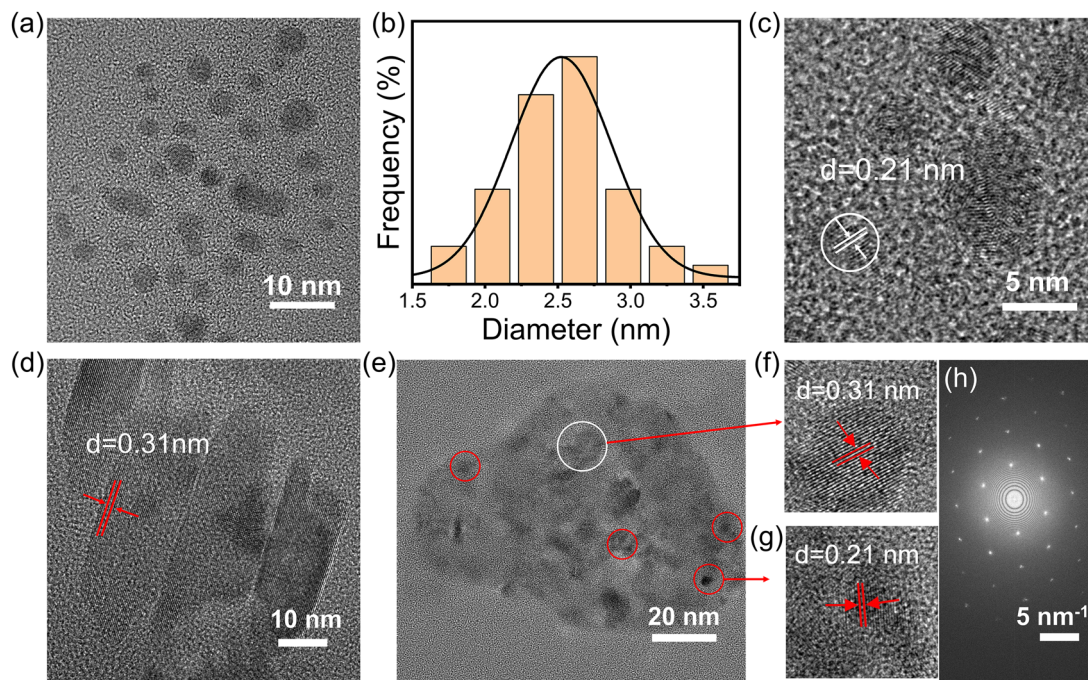This journal is © The Royal Society of Chemistry 2022

Fig. 1 (a) TEM and (c) HRTEM images of g-CDs. (b) Size distribution of the g-CDs. (d) HRTEM image of UiO-66. (e) TEM and (f and g) HRTEM images of g-CDs@UiO-66. (h) SAED pattern of g-CDs@UiO-66.
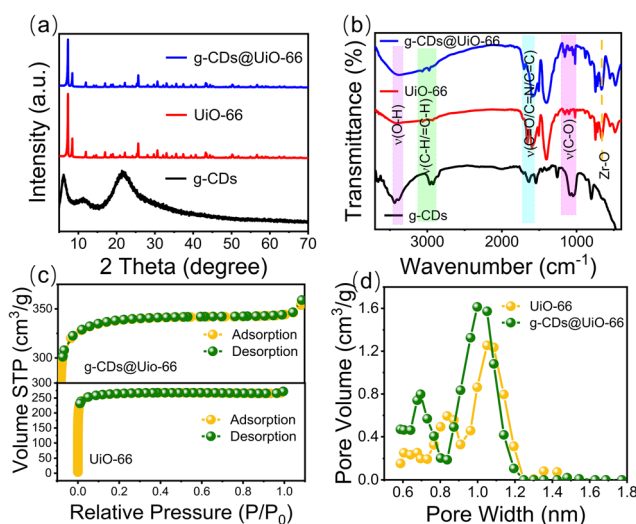

Fig. 2 (a) XRD patterns of the g-CDs (black line), UiO-66 (red line), and g-CDs@UiO-66 (blue line). (b) FT-IR spectra of the g-CDs, UiO-66, and g-CDs@UiO-66. (c) N_2 adsorption–desorption isotherms, and (d) pore volume distributions of UiO-66 and g-CDs@UiO-66.

These bands were ascribed to O–H, C–H/=C–H, C=O/C=N, C=C, C=O, and Zr–O stretching vibrations, respectively.[37] All of these characteristic peaks are found in g-CDs@UiO-66, which presents strong proof of the presence of g-CDs and UiO-66 in the g-CDs@UiO-66 composite. In addition, after adding g-CDs, the C=N/C=O and C–O peaks of the original UiO-66 are increased, probably due to new bonds formed between the g-CDs and UiO-66.

Fig. 2c shows the N_2 adsorption and desorption isotherms. It can be seen that both UiO-66 and g-CDs@UiO-66 are I-type

isotherm curves, indicating the presence of microporosity. As shown in Fig. 2d, g-CDs@UiO-66 still maintained the microporous structure of UiO-66 upon doping with g-CDs. However, since g-CDs occupy part of the pores, the volume of the pores decreases a little.[38] Similar results were observed for the Brunauer–Emmett–Teller specific surface area (Table S1, ESI†). The specific surface area of g-CDs@UiO-66 increased from 1035 m^2 g^{-1} (UiO-66) to 1343 m^2 g^{-1},[39] further proving that the synthesis of g-CDs@UiO-66 is not entirely electrostatic and that the high specific surface area provides a large adsorption site for NFX.

XPS spectra were further measured to investigate the chemical composition of UiO-66 and g-CDs@UiO-66. In Fig. 3a, the main elements appearing in the XPS spectrum of UiO-66 are C, O, and Zr. Fig. 3b shows the C 1s spectrum of UiO-66. The spectrum of C 1s comprises three individual component peaks, which are C=O (288.18 eV), C–O (285.88 eV), and C–C (284.18 eV).[33] The binding energy of C=O was increased after the addition of g-CDs compared with the original. This may be due to the interaction between the organic binders during the complexation of g-CDs with UiO-66.[33] The high-resolution spectrum of O 1s presented two peaks at 531.48 eV and 533.08 eV in UiO-66, indicating the existence of different chemical states of oxygen, respectively referred to adsorbed oxygen (O_{ads}) and surface hydroxyl (O_{OH}).[40] In addition, the addition of g-CDs does not cause a shift in the O_{ads} peak, but the peaks of O_{OH} are red-shifted, meaning that the addition of g-CDs may affect the detection of norfloxacin.[33] The Zr 3d spectrum of the g-CDs@UiO-66 composite has two peaks, at 182.18 eV and 184.48 eV, which can be ascribed to Zr $3d_{5/2}$ and Zr $3d_{3/2}$, respectively.[41] This further proves that the doping of g-CDs is connected *via* chemical bonding.
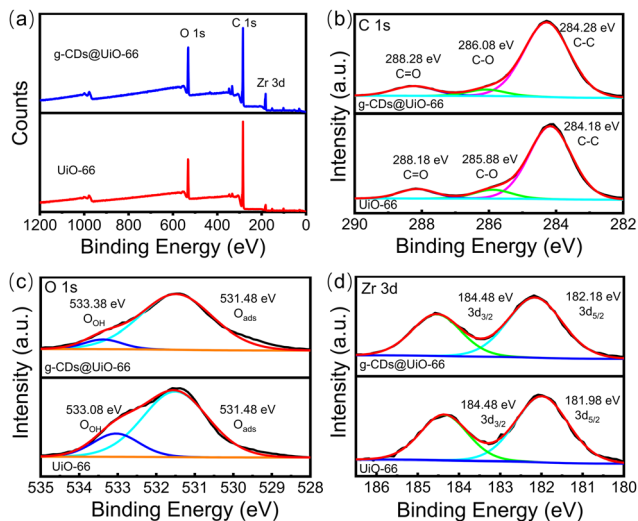
Fig. 3 (a) XPS spectra of UiO-66 (red line) and g-CDs@UiO-66 (blue line), and high-resolution spectra of (b) C 1s, (c) O 1s, (d) Zr 3d.

Optical properties

The fluorescence characteristics of g-CDs, UiO-66, and g-CDs@UiO-66 were further studied. As shown in Fig. 4a, only UiO-66 has a weak fluorescence intensity at 375 nm. g-CDs have a strong fluorescence band at 536 nm (Fig. 4b). To further explore the photometric properties of g-CDs@UiO-66, the UV-vis absorption spectra and the photoluminescence spectra of g-CDs in ethanol were studied. As displayed in Fig. 4b, the ultraviolet absorption spectrum of g-CDs shows four obvious absorption peaks, located at 217, 260, 350, and 447 nm, respectively, representing the $\pi \rightarrow \pi^*$ transition of aromatic C=C bonds[42,43] and the $n \rightarrow \pi^*$ transition of the aromatic sp^2 system including C=O.[44] When g-CDs and UiO-66 are combined, the resulting
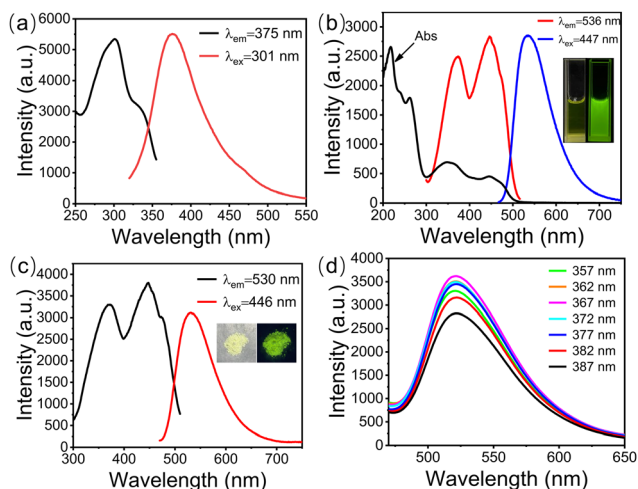

Fig. 4 (a) Fluorescence spectra of UiO-66. (b) UV-vis absorption and FL spectra of g-CDs in aqueous solution. The inset shows a photograph of g-CDs under sunlight (Left) and UV light (Right). (c) FL spectra of g-CDs@UiO-66. The inset shows a photograph of g-CDs@UiO-66 under sunlight (Left) and UV light (Right). (d) g-CDs@UiO-66 emission spectra at different excitation wavelengths.

g-CDs@UiO-66 is pale yellow under visible light, but strongly green under 365 nm UV light (inset Fig. 4c). The highest emission at 530 nm can be obtained with excitation at 446 nm (Fig. 4c). Furthermore, the emission spectra of g-CDs@UiO-66 under different excitations (Fig. 4d) were recorded. The fluorescence emission wavelength of g-CDs@UiO-66 is independent of the excitation wavelength. This excellent photoluminescence performance shows the potential of g-CDs@UiO-66 as a luminescent sensing probe.

Sensing performance for norfloxacin

The detection of actual samples is also subject to selectivity, which is a aspect that must be considered. The fluorescence response of g-CDs@UiO-66 to different metal ions and representative antibiotics (including Ca^{2+}, Na^+, K^+, Mg^{2+}, Fe^{3+}, Cu^{2+}, glutamic acid, histidine, cysteine, tryptophan, amoxicillin, ampicillin, erythromycin, chloramphenicol, tetracycline, and norfloxacin) at concentrations of 10^{-4} mol L^{-1} was studied. As displayed in Fig. 5a, the addition of norfloxacin increased its fluorescence intensity (while the addition of other substances had almost no influence on the fluorescence intensity).[2] Fig. 5b shows the emission-intensity changes of the sensing probes in the presence of representative antibiotics, heavy metal ions, and acids as interfering substances. It can be seen that other interfering substances do not affect the response when coexisting with NFX. These results demonstrated that the effects of other interferents were negligible and that g-CDs@UiO-66 showed good selectivity for NFX.

Under the optimized experimental conditions (λ_{ex} = 380 nm), the sensitivity, linear response range, and detection limit of the
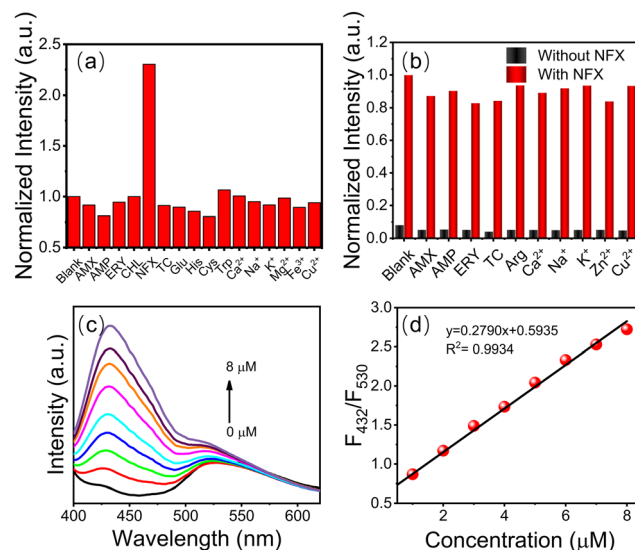

Fig. 5 (a) Ratio of fluorescence intensity (F/F_0) for g-CDs@UiO-66 in the presence of various antibiotics, metal ions, and amino acids. (F and F_0 are the fluorescence intensity at 432 nm in the presence and absence of norfloxacin, respectively.) (b) Fluorescence intensity response (F/F_0) of g-CDs@UiO-66 to norfloxacin in the presence of different interfering substances (530 nm). (c) FL spectra of g-CDs@UiO-66 in different concentrations of norfloxacin. (d) Linear relationship between F_{432}/F_{530} and NFX concentration.

15512 | *J. Mater. Chem. C*, 2022, **10**, 15508–15515

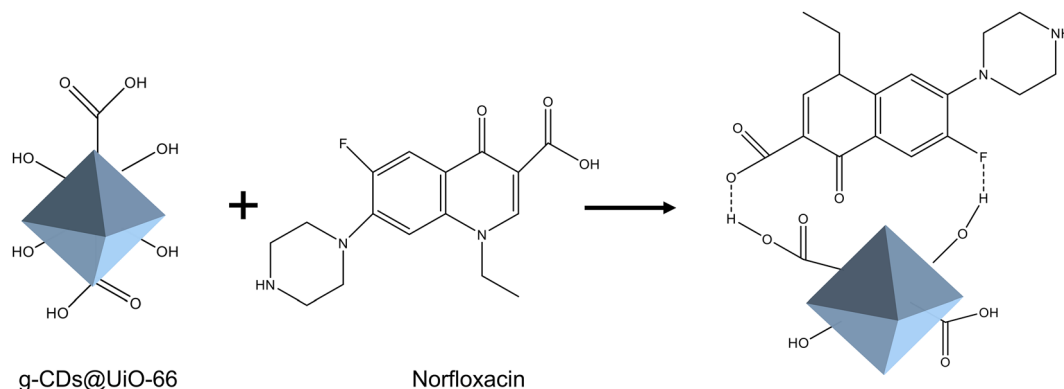This journal is © The Royal Society of Chemistry 2022

Fig. 6   Possible mechanism of interaction between g-CDs@UiO-66 and NFX.

g-CDs@UiO-66 sensing system were measured. By performing FL enhanced titrations *via* adding g-CDs@UiO-66 to different concentrations of norfloxacin aqueous solutions, it was found that a dose-dependent interaction existed between the FL response (F_{432}/F_{530}) and the norfloxacin concentration. The emission intensity of g-CDs@UiO-66–NFX gradually increases as the norfloxacin concentration is increased (Fig. 5c). The fluorescence ratio (F_{432}/F_{530}) of norfloxacin in the concentration range of 1–8 μM shows a good linear correlation with the concentration (R^2 = 0.9934) (Fig. 5d). The detection limit (LOD) of norfloxacin calculated from 3σ/slope is 0.082 μM. Compared with other reported methods of detecting norfloxacin,[45–47] the g-CDs@UiO-66 sensing system has a higher sensitivity to norfloxacin.

Possible fluorescence-enhancement mechanism of norfloxacin and g-CDs@UiO-66

To better understand the enhancing effect of norfloxacin on the luminescence of g-CDs@UiO-66, its possible fluorescence-enhancement mechanism was researched. The mechanism of fluorescence enhancement may be as follows. As depicted in Fig. 2b, the composite surface is rich in hydroxyl groups and carboxyl groups. On the one hand, the surface of NFX is rich in C–F, C=O, C–N, and COOH groups. When NFX and g-CDs@UiO-66 approach each other, they form strong hydrogen-bond

interactions (Fig. 6).[2] Thus, the presence of strong hydrogen bonds leads to fluorescence enhancement. On the other hand, the electrostatic repulsion between the NFX adsorbed on the surface of g-CDs@UiO-66 would increase the distance between the g-CDs@UiO-66 particles, which would effectively separate the g-CDs@UiO-66 particles from each other, and further reduce the non-radiative decay.[48] In addition, the attachment of NFX could potentially vary the surface defects of g-CDs@UiO-66, leading to an enhancement of the PL intensity.[49]

A further study was conducted to understand the fluorescence-enhancement phenomenon better. Firstly, g-CDs@UiO-66 can form hydrogen bonds when mixed with substances including C–F, C–OH, C–N, and COOH, resulting in the enhanced fluorescence intensity of g-CDs@UiO-66.[2,50] Secondly, the FT-IR spectrum of g-CDs@UiO-66 after NFX immersion showed the vibration for C–OH around 3370 cm^{-1} (Fig. 7a), which was red-shifted by 50 cm^{-1} relative to the unsoaked g-CDs@UiO-66 (3420 cm^{-1}).[51] Furthermore, norfloxacin itself may be responsible for the enhanced fluorescence. Fig. 7b shows that the g-CDs@UiO-66–NFX system had a higher fluorescence intensity than the separate g-CDs@UiO-66 and NFX systems. Moreover, the surface of g-CDs@UiO-66 is positively charged (+5.8 mV), while the surface of NFX is negatively charged, indicating a good electrostatic attraction between the g-CDs@UiO-66 composite and NFX.[29] On the basis of the above discussions, it is
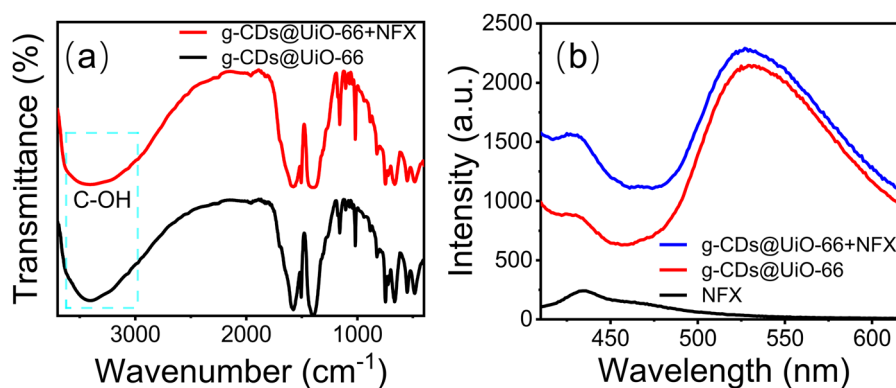

Fig. 7   (a) FT-IR spectra of g-CDs@UiO-66 before and after immersion in NFX, and (b) PL spectra of g-CDs@UiO-66, NFX and the g-CDs@UiO-66–NFX system with an NFX concentration of 10^{-4} mol L^{-1}.

This journal is © The Royal Society of Chemistry 2022

J. Mater. Chem. C, 2022, **10**, 15508–15515 | **15513**

Table 1 Determination of NFX content in real samples (*n* = 3)

Samples	Spiked (μM)	Found (μM)	Recovery (%)	RSD (%)
Milk	3	2.96	98.6 ± 1.5	1.5
	6	6.03	100.5 ± 3.1	3.1
Pork	3	3.14	104.6 ± 3.2	3.2
	6	5.85	97.5 ± 1.9	1.9

thought that the enhancement of fluorescence for g-CDs@UiO-66 may be due to the hydrogen-bonding action between g-CDs@UiO-66 and NFX.

Application in real samples

To demonstrate the feasibility of this fluorescent sensing material for detecting NFX in actual samples, the recovery was determined using the standard addition method.[52] In the recovery rate test of standard additions in the actual sample, the recovery rate of the sample measurement was between 97.5–101.6% (Table 1). These results demonstrate the reliability and accuracy of the fluorescent sensing material in detecting actual samples.

Conclusions

In this work, a novel MOF-based g-CDs@UiO-66 composite was prepared successfully *via* stirring. The fluorescent composite not only maintains good fluorescence and structural stability in aqueous solution but also shows the excellent optical properties of g-CDs and UiO-66, making it an excellent probe for the fluorescence detection of norfloxacin. The fluorescent sensing material has both the outstanding optical properties of the g-CDs and the selective detection and clearance capability of UiO-66 for the target analyte, which can be applied to the detection of norfloxacin in milk and pork samples. In addition, the synthesized g-CDs@UiO-66 nanoparticles, as a fluorescent sensing material for the detection of norfloxacin, demonstrate high sensitivity and specificity, where the detectability is as low as 0.082 μM for the detection range of 1–8 μM. The results of this study will help to promote the combination of carbon dots and MOF, and provide a new avenue for the development of carbon dot–metal–organic framework composite sensing technologies in the field of pesticide residue detection in food and the environment.

Conflicts of interest

The authors declare no competing financial interest.

Acknowledgements

Notes and references

1 L. Chen, D. Liu, J. Peng, Q. Du and H. He, *Coord. Chem. Rev.*, 2020, **404**, 213113.
2 M. Yang, H. Li, J. Liu, W. Kong, S. Zhao, C. Li, H. Huang, Y. Liu and Z. Kang, *J. Mater. Chem. B*, 2014, **2**, 7964–7970.
3 B. Prutthiwanasan, C. Phechkrajang and L. Suntornsuk, *Talanta*, 2016, **159**, 74–79.
4 K. Chaiyasing, B. Liawruangrath, S. Natakankitkul, S. Satienperakul, N. Rannurags, P. Norfun and S. Liawruangrath, *Spectrochim. Acta, Part A*, 2018, **202**, 107–114.
5 Y. Zhang, Y. Xie, C. Zhang, M. Wu and S. Feng, *J. Sep. Sci.*, 2020, **43**, 478–485.
6 B. Deng, C. Su and Y. Kang, *Anal. Bioanal. Chem.*, 2006, **385**, 1336–1341.
7 K. Huang, X. Liu, W. Xie and H. Yuan, *Colloids Surf., B*, 2008, **64**, 269–274.
8 W. Lu, J. Liu, J. Li, W. Wang, M. Lv, R. Cui and L. Chen, *Analyst*, 2019, **144**, 1292–1302.
9 W. Wang, X.-H. Xiong, N.-X. Zhu, Z. Zeng, Z.-W. Wei, M. Pan, D. D. Fenske, J.-J. Jiang and C.-Y. Su, *Angew. Chem.*, 2022, **61**, e202201766.
10 Y.-H. Zou, Y.-B. Huang, D.-H. Si, Q. Yin, Q.-J. Wu, Z. Weng and R. Cao, *Angew. Chem.*, 2021, **60**, 20915–20920.
11 X. Sun, K. Yuan and Y. Zhang, *J. Rare Earths*, 2020, **38**, 801–818.
12 S. Han, Y. Song, S. Liu, L. Zhao and R. Sun, *Eur. Polym. J.*, 2022, **171**, 111219.
13 T. Lu, L. Zhang, M. Sun, D. Deng, Y. Su and L. Lv, *Anal. Chem.*, 2016, **88**, 3413–3420.
14 C. Gu, Y. Ding, X. Quan, M. Gong, J. Yu, D. Zhao and C. Li, *J. Rare Earths*, 2021, **39**, 1024–1030.
15 Y.-H. Li, C.-C. Wang, X. Zeng, X.-Z. Sun, C. Zhao, H. Fu and P. Wang, *Chem. Eng. J.*, 2022, **422**, 136276.
16 N. Patel, P. Shukla, P. Lama, S. Das and T. Pal, *Cryst. Growth Des.*, 2022, **22**, 3518–3564.
17 J. Peng, W. Zhou, H. Ding, H. Du and S. Li, *J. Rare Earths*, 2021, **39**, 446–452.
18 B. Li, T. Suo, S. Xie, A. Xia, Y.-J. Ma, H. Huang, X. Zhang and Q. Hu, *Trac-Trend Anal. Chem.*, 2021, **135**, 116163.
19 J. Roghayeh, I.-N. Mahsa Haddad, K. Alireza and W. Sang, *Spectrochim. Acta, Part A*, 2021, **262**, 120089.
20 Y. Tao, Y. Jiang, Y. Huang, J. Liu, P. Zhang, X. Chen, Y. Fan and L. Wang, *CrystEngComm*, 2021, **23**, 4038–4049.
21 H. Zhang, Y. Li, H. Lu and F. Gan, *Anal. Bioanal. Chem.*, 2022, **414**, 2471–2480.

15514 | *J. Mater. Chem. C*, 2022, **10**, 15508–15515

This journal is © The Royal Society of Chemistry 2022

22 D. Li, H. He, H. Zhang, X. Yang, Y. Kang, R. Dong, W. Li, X. Pan, E. Kou, Y. Liu and B. Lei, *Chin. J. Lumin.*, 2021, **42**, 635–641.

23 Y. Li, X. Xu, W. Li, C. Hu, J. Zhuang, X. Zhang, B. Lei and Y. Liu, *Chin. J. Lumin.*, 2021, **42**, 1172–1181.

24 J. Liu, Y. Geng, D. Li, H. Yao, Z. Huo, Y. Li, K. Zhang, S. Zhu, H. We, W. Xu, J. Jiang and B. Yang, *Adv. Mater.*, 2020, **32**, 1906641.

25 W. Li, G. S. Schierle, B. Lei, Y. Liu and C. F. Kaminski, *Chem. Rev.*, 2022, **122**, 12495–12543.

26 J. Yue, L. Li, C. Jiang, Q. Mei, W.-F. Dong and R.-H. Yan, *J. Mater. Chem. B*, 2021, **9**, 7972–7978.

27 T. Islamoglu, K.-I. Otake, P. Li, C. Buru, A. Peters, I. Akpinar, S. Garibay and O. Farha, *CrystEngComm*, 2018, **20**, 5913–5918.

28 Z. Lu, J. Liu, X. Zhang, Y. Liao, R. Wang, K. Zhang, J. Lyu, O. Farha and J. Hupp, *J. Am. Ceram. Soc.*, 2020, **142**, 21110–21121.

29 R. Han, N. Zheng, Z. Yu, J. Wang, X. Xu, X. Qu, S. Li, Y. Zhang and J. Wang, *Food Chem.*, 2015, **181**, 119–126.

30 Y. Ma, X. Han, S. Xu, Z. Wang, W. Li, I. Silva, S. Chansai, D. Lee, Y. Zou, M. Nikiel, P. Manuel, A. Sheveleva, F. Tuna, E. McInnes, Y. Cheng, S. Rudić, A. Ramirez-Cuesta, S. Haigh, C. Hardacre, M. Schröder and S. Yang, *J. Am. Chem. Soc.*, 2021, **143**, 10977–10985.

31 Y. Xu, Y. Lin, N. Chu, Y. Xing and X. Chen, *Chem. Eng. J.*, 2022, **435**, 134907.

32 J. Chen, W.-R. Liu, Y. Li, X. Zou, W. Li, J. Liang, H. Zhang, Y. Liu, X. Zhang, C. Hu and B. Lei, *Chem. Eng. J.*, 2022, **428**, 131168.

33 J. Yu, X. Wang, L. Chen, G. Lu, G. Shi, X. Xie, Y. Wang and J. Sun, *Chem. Eng. J.*, 2022, **435**, 135033.

34 C. Lin, K. Sun, C. Zhang, T. Tan, M. Xu, Y. Liu, C. Xu, Y. Wang, L. Li and A. Whittaker, *Microporous Mesoporous Mater.*, 2022, **293**, 109775.

35 H. Li, M. Fu, S.-Q. Wang, X. Zheng, M. Zhao, F. Yang, C. Tang and Y. Dong, *Environ. Sci. Technol.*, 2021, **55**, 14917–14927.

36 J. Chen, J. Ouyang, W. Chen, Z. Zheng, Z. Yang, Z. Liu and L. Zhou, *Chem. Eng. J.*, 2022, **431**, 134045.

37 J.-X. Li, G.-G. Chang, G. Tian, C. Pu, K.-X. Huang, S.-C. Ke, C. Janiak and X.-Y. Yang, *Adv. Funct. Mater.*, 2021, **31**, 2102868.

38 L. Chen, X. Wang, Z. Rao, Z. Tang, Y. Wang, G. Shi, G. Lu, X. Xie, D. Chen and J. Sun, *Chem. Eng. J.*, 2021, **416**, 129112.

39 Y. Wang, B. Wang, H. Shi, C. Zhang, C. Tao and J. Li, *Inorg. Chem. Front.*, 2018, **5**, 2739–2745.

40 F. Bi, X. Zhang, J. Chen, Y. Yang and Y. Wang, *Appl. Catal., B*, 2020, **269**, 118767.

41 F. Yang, J. Ma, Q. Zhu, Z. Ma and J. Wang, *ACS Appl. Mater. Interfaces*, 2022, **14**, 22510–22520.

42 H. Guo, X. Wang, N. Wu, M. Xu, M. Wang, L. Zhang and W. Yang, *Anal. Chim. Acta*, 2021, **1141**, 13–20.

43 C. Singaravelu, X. Deschanels, C. Rey and J. Causse, *ACS Appl. Nano Mater.*, 2021, **4**, 6386–6397.

44 R. Dong, Y. Yao, D. Li, H. Zhang, W. Li, M. Molokee, Y. Liu and B. Lei, *Sens. Actuators, B*, 2020, **321**, 128643.

45 S. Chen, X. Su, C. Yuan, C. Q. Jia, Y. Qiao, Y. Li, L. He, L. Zou, X. Ao, A. Liu, S. Liu and Y. Yang, *Spectrochim. Acta, Part A*, 2021, **253**, 119577.

46 N. Yang, Q.-L. Wen, Y.-B. Fu, L.-F. Long, Y.-J. Liao, S.-B. Hou, P. Qian, P. Liu, J. Ling and Q. Cao, *Spectrochim. Acta, Part A*, 2022, **281**, 121568.

47 Q.-L. Cao, L. Fu and G.-H. Cui, *J. Solid State Chem.*, 2022, **313**, 123330.

48 K. Wang, Q. Ji, J. Xu, H. Li, D. Zhang, X. Liu, Y. Wu and H. Fan, *J. Fluoresc.*, 2018, **28**, 759–765.

49 J. Niu and H. Gao, *J. Lumin.*, 2014, **149**, 159–162.

50 C. Lu, G. Liu, Z. Yang, Y. Wang, H. Rao, W. Zhang, B. Jing and X. Wang, *Microchim. Acta*, 2020, **187**, 37.

51 Q. Qu, A. Zhu, X. Shao, G. Shi and Y. Tian, *Chem. Commun.*, 2012, **48**, 5473–5475.

52 T. Liu, J. He, Z. Lu, M. Sun, M. Wu, X. Wang, Y. Jiang and P. Zou, *Chem. Eng. J.*, 2022, **429**, 13246.1.